Uncertainty Evaluation of the Unified Method for Thermo-Electric Module Characterization

Uncertainty Evaluation of the Unified Method for Thermo-Electric Module Characterization

G.M. D'Aucelli, N. Giaquinto, C. Guarnieri Calò Carducci, M. Spadavecchia, A. Trotta

Abstract

In this paper the uncertainty evaluation of the recently proposed Unified Method for Thermo-Electric Module characterization is carried out. The measurement model is detailed and individual uncertainty contributions are highlighted, with close reference to the instrumentation and measurement setup. The uncertainty evaluation is performed by means of a Monte Carlo Simulation. The same algorithm is used to perform a sensitivity analysis, giving a comprehensive insight into the most critical issues of the proposed method and assessing the performance of the two adopted electrical stimuli. The experimental results thereby obtained are discussed and improvements to the measurement setup and technique are finally proposed.

Keywords: Thermoelectric devices, Estimation, Monte Carlo methods, Measurement uncertainty, Sensitivity analysis

1. Introduction

Thermoelectricity is an emerging technology capable of harvesting electrical energy from waste heat, thus potentially increasing the energy-efficiency in many applications ranging from aerospace [1–3], to industrial ones [4–7] with low environmental impact.

Thermo-Electric Modules (TEMs), due to their high reliability and compactness, are well suited to work alongside other energy harvesting technologies

Email addresses: giuseppemaria.daucelli@poliba.it (G.M. D'Aucelli), nicola.giaquinto@poliba.it (N. Giaquinto), cguarnieri@eonerc.rwth-aachen.de (C. Guarnieri Calò Carducci), maurizio.spadavecchia@poliba.it (M. Spadavecchia), amerigo.trotta@poliba.it (A. Trotta)

such as photovoltaic [8, 9], to recover the otherwise dissipated heat from the rear of solar panels. As generator, a TEM or an array of TEMs, could be also a valid alternative to batteries in giving an autonomous source of energy to sensor nodes [10–12] and wireless sensor networks [2, 9, 13, 14]. TEMs have also been extensively considered, as heating/cooling devices, to control the operating temperature of microelectronic devices to allow higher clock rates [15], in air conditioning systems [16] and for refrigeration applications [4, 17].

Performances of TEMs are generally given from manufacturers in some standard operating conditions (for example at maximum heat flux) but, in real applications, a TEM-based system rarely works at such conditions. For this reason, since a couple of years, a great research effort is being directed into TEM performance assessment under a broader range of ambient temperature and heat fluxes [18–21].

A typical specification provided by TEM manufacturers is the largest temperature difference ΔT_{max} obtainable between the two faces of the module when cooling capacity is zero at cold side. This parameter is often specified in correspondence of no more than a couple of hot side temperature values (for instance 300 K and 323 K) [22]. Conversely, when the TEM is designed for energy harvesting, the power, voltage and maximum efficiency at matched load condition (i.e. load resistance equals the internal electrical resistance of the module R_{in}) are usually given. Clearly, all the values provided as product specifications are related only to ideal use cases and merely useful as general design criteria, but heavily inaccurate in most real applications.

In a recent work, the authors have developed a testbed to perform an Unified Method (UM) to quickly estimate the TEM's equivalent electrical and thermal model parameters, i.e. the Seebeck coefficient α_S, the internal electric resistance R_{in} and the thermal equivalent resistance Θ_{in}, in a wide range of temperature differences, ambient temperatures and electric loads [23]. In [23], two different current profiles, namely Current Sweep (CS) and Small Signal (SS) were applied to the TEM to derive all the parameters in a single test, using a quite simple configuration. In that paper a first analytical comparison among the standard uncertainties obtained from the two proposals has been reported. The uncertainty assessment was based on the study of the linear regression problem in determining the internal resistance R_{in} and the Seebeck voltage V_{th} whereas the uncertainty on the estimation of the Θ_{in} was evaluated by applying the standard uncertainty propagation proposed by the Guide to the Expression of Uncertainty in Measurement (GUM) [24]. The application of the GUM approach is straightforward, however its application to the sensitivity analysis requires calculating the sensitivity coefficients through partial derivatives of the measurement model [25]. In most practical cases, the correlation coefficients and high-order uncertainty components are supposed negligible [26], but still the complexity of the measurement model makes this approach unfeasible. As better justified in Section 4, a good alternative to the GUM method are Monte Carlo (MC) simulations, like those described in [27], and [28]. The method simulates a high number of measurements by randomly sampling all input quantities from known probability distributions, thus numerically obtaining the distributions of output quantities by straightforwardly applying the measurement model [25, 29].

In [30] all uncertainty sources are identified for both electrical resistivity and Seebeck coefficient; the former was measured using a potentiometric configuration, and the latter by applying the differential Seebeck method. As probes, two thermocouples mechanically clamped on the sample were used. The test was conducted in a furnace with temperature ranging from room temperature up to 1200 K, whereas ΔT was varied from 0 up to 10 K using a heater. Using the GUM approach, the authors have obtained, for the Seebeck coefficient, a temperature dependent and asymmetric uncertainty between $+1.0\%$ and -13.1% of the nominal value at high temperature and $\pm1.0\%$ near room temperature. The electrical resistivity was determined to be $\pm7.0\%$ across any measurement temperature [30].

A similar approach was applied in [31] where uncertainties less than 5% and 4% were found for the measurement of the Seebeck coefficient and electrical resistivity respectively, but the characterization was made near room temperature with a small temperature gradient (~ 3 K). Another uncertainty analysis of a thermoelectric materials characterization procedure near room temperature can be found in [32], where some of the measurement systems developed at Fraunhofer Institute for Physical Measurement Techniques are summarized and a 10% accuracy is estimated for Seebeck coefficient, electrical conductivity and thermal conductivity, whereas the uncertainty for the measurement of the figure of merit was estimated to about 40%.

Whereas the aforementioned works are mainly oriented to describe, in terms of uncertainty, only the electrical parameters in samples of bulk thermoelectric materials, this paper focuses on the detailed uncertainty evaluation and on the sensitivity analysis to individual input uncertainties of both electrical and thermal parameters of a TEM.

In Section 2, the mathematical models with the main inputs, outputs and the UM are described, pointing out the advantages introduced by the proposed method. Afterwards, in Section 3, the testbed for electrical and thermal characterization is briefly outlined and the uncertainty contributions from each source and known parameters are detailed. In Section 4 the approach to the metrological characterization of the proposed technique is introduced by specifying the input uncertainty contributions considered in the Monte Carlo Simulation and explaining how the sensitivity of each output quantity to such contributions has been assessed. Finally, in Section 5, experimental results are presented and, consequently, conclusions are drawn.

2. The TEM Unified Method

To characterize the electrical behavior of a TEM, the Seebeck coefficient α_S and the internal resistance R_{in} must be estimated. The whole measurement procedure is outlined in Figure 1. First, the Kirchhoff's voltage law at the terminals of the module can be considered:

$$V = R_{in} I + \alpha_S \Delta T \tag{1}$$

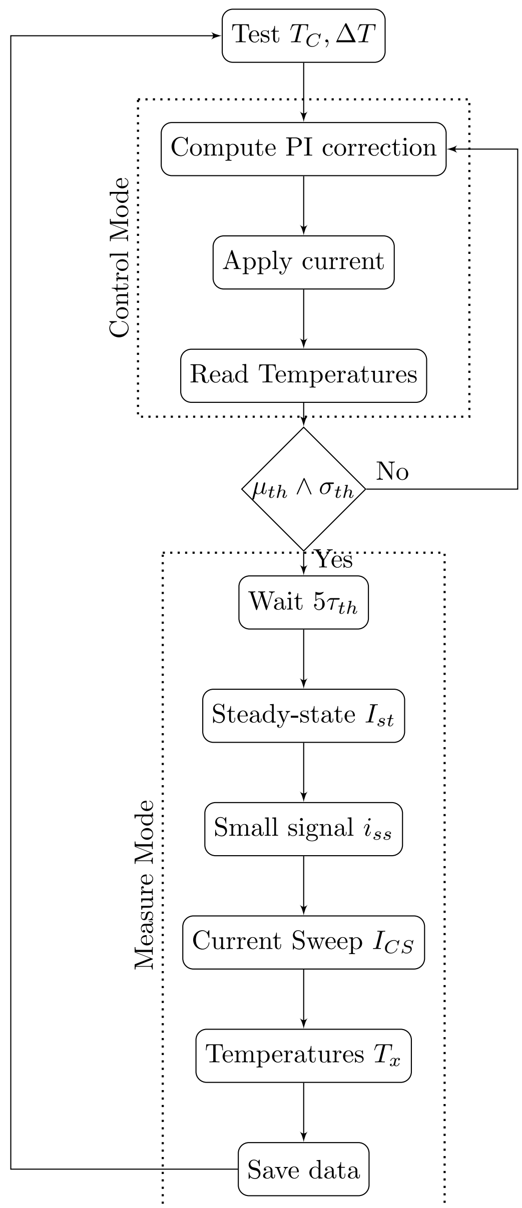

Figure 1: Measurement process flow chart

Conversely, the thermal behavior of a TEM can be described by the thermal resistance Θ_{in} of the module. Its value is derived by measuring the emitted and absorbed heat fluxes q_{em} and q_{abs}, and solving the energy balance between the Peltier effect, the heat conduction and the Joule effect, averaging the respective equations

$$\begin{cases} q_{em} = \alpha_S I T_h - \frac{T_h - T_c}{\Theta_{in}} + \frac{I^2 R_{in}}{2} \\ q_{abs} = \alpha_S I T_c - \frac{T_h - T_c}{\Theta_{in}} - \frac{I^2 R_{in}}{2} \end{cases} \tag{2}$$

where T_h and T_c are, respectively, the temperature of the hot and cold side.

The thermoelectric performance relies directly on the dimensionless thermoelectric figure of merit $Z\bar{T}$ which summarizes the bulk material properties and allows comparisons between different TEMs.

$$Z\bar{T} = \frac{\alpha_S^2 \Theta_{in}}{R_{in}} \bar{T} \tag{3}$$

where $\bar{T}$ is the average temperature between the hot and the cold side of the module, as defined in Section 3.1.

From equation (3), $Z\bar{T}$ is a function of the electrical resistance, the Seebeck-coefficient and the thermal resistance and can be determined by measuring α_S, R_{in} and Θ_{in} separately [33] or directly using the Harman Method (HM) [34] or other transient methods [35]. An example of direct measurement of the Figure of Merit is the "Z meter", a technique for rapid pass/fail test of TEMs with moderate accuracy [36].

However, all three quantities in (3) give information about electric and thermal processes in a material. Consequently, in thermoelectric research but also in commercial devices, it is most common to estimate each parameter individually to obtain the figure of merit and to determine the transport properties of material samples. It is to be noted that the HM can only be carried out under small temperature differences.

For example, α_S and Θ_{in} are usually measured under a temperature difference of $10 - 20$ K without an electric current flowing through the material sample, while R_{in} is measured at isothermal conditions by applying a small excitation current (in the order of a few milliamperes) [33]. Similarly, the HM is only valid if the Joule heat generation is negligible, thus a weak current and a small temperature difference should be imposed [34].

Generally, a TEM is usually operated under much larger temperature differences, with significant electric currents flowing in the module; this is the case of the characterization of thermoelectric power generators. In such scenarios, the above-mentioned techniques do not provide measurement results relevant to actual operating conditions.

A lot of research has already been published reporting characterization techniques for TEMs under such operating conditions [37–39]. However, the presented techniques adopt complex setups, requiring mechanical components to compress the test stack and a combination of heat sink/sources with both vacuum and circulating pumps to keep the thermal gradient constant and to avoid heat dissipation phenomena. A comprehensive survey of different approaches and testbeds is given in [40].

Another interesting procedure implementing a transient method is proposed by McCarty [41], where a V–I curve tracing method is described that estimates also the average thermal resistance of a TEM. This method requires only four data points obtained by switching a relay (short circuit condition, open circuit condition and the two transitions at near thermal steady state). No reproducibility nor accuracy information is, however, provided for the method.

The UM for TEM characterization has been introduced to overcome the limitations of the previous methods. Using this method, it is possible to fully characterize a TEM in two different quadrants of the $P-I$ plane, i.e. in both energy-generating and heating-cooling mode [42] with a good accuracy. Many different operating conditions, typical in temperature control scenarios, can be explored by setting the room temperature T_a (i.e. the cold side temperature of the TEM) and the temperature difference ΔT between the two sides. Measured module parameters can then be used to accurately simulate TEM performance in real life scenarios.

The UM is based on a measurement scheme whose complexity can be adapted according to the required uncertainty or to the available instrumentation, using two different measurement techniques. As detailed in [23], the UM, constist in applying first a constant current to reach a given steady state, which results in a temperature difference ΔT between the two sides obtained using a Proportional-Integrative (PI) controller in a closed-loop feedback; then, a stimulus signal is applied and the resulting current flowing in the module and voltage at its terminal are acquired. Two different stimuli are proposed:

- the *small signal* (SS) consists in sinusoidal stimulus with an amplitude of approximately 12 mA that is added to the steady state current. It requires no previous assumption and is generally faster because the bias point is not altered. This stimulus requires a simple power driver, but produces worse results in terms of uncertainty for increasing values of ΔT;
- the *sweep signal* consists in a current sweep (CS) from the bias value to its opposite. It requires a previous identification of the dynamic model of the module and a 4-quadrant power amplifier, but produces far more better results in terms of accuracy.

3. Experimental setup

The above described steps have been implemented in an automatic test procedure that carries out measurements over customizable combinations of the cold side temperature T_c and the working ΔT. This last parameter is, in particular, set by imposing a steady state current I_{st} to the TEM and exploiting the Peltier effect. The whole test was conducted inside a Discovery Es 250 (DY-250) climate chamber by Angelantoni Group S.p.A., that brings the cold side of the module to the ambient temperature. The developed testbed automatically sweeps along a wide range of electrical load conditions using only a DAQ board and a 4-quadrant transconductance amplifier as shown in Figure 2.

Measurements for thermal characterization have been performed by using two heat flux sensors. Each one was implemented by means of three layers:

- Aluminum (2 mm)

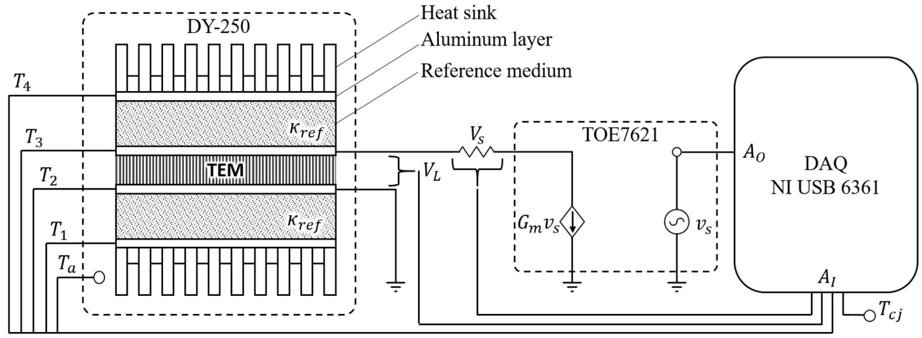

Figure 2: Synoptic diagram of the measurement system for the UM

- Glass (8 mm)
- Aluminum (2 mm)

Metal layers have been equipped with J-type thermocouples inserted in suitably drilled holes. A thin layer of high thermal conductivity silver-based thermal paste was interposed between layers to minimize the thermal contact resistance.

3.1. Setup and Measurement Model

The proposed method consists in placing the TEM under test between two heat-flux sensors (Figure 2); when the desired operating conditions are met, i.e. when the thermal steady state has been reached, the driving current is locked to the last current value, and the supervisory software waits for all transients to run out. Then, the SS profile is applied: a small 10 Hz sinusoidal current stimulus is added to the steady state current I_{st}; finally, the CS profile is applied and the driving current I_{st} is swept to its symmetric value $-I_{st}$ with a ramp-like signal. The duration of each described current profile is set to a value that is sufficiently low with respect to the thermal time constant of the module [23]. When the test procedure is completed, the following quantities are obtained: the temperatures at each layer, the voltage V_L and the current I at its terminals.

At the end of each test, all raw data (acquired voltages) are stored for further post-processing in MATLAB environment:

- V_L is not processed

- V_s is divided by R_s to obtain I. R_s is a 1 $\Omega \pm 0.0035\%$ shunt resistor measured with an Agilent 3458A $8^{1/2}$ digital multimeter in 4-wires configuration

- T_a and T_{cj} are obtained from respective voltages using two LM35A integrated thermal sensors by Texas Instruments, with nominal sensitivity $S = 10$ mV/(K)

- T_1, T_2, T_3, T_4 are computed using NIST coefficients for J-type thermocouples and applying a software cold-junction compensation as described in subsection 3.4

- q_{em} and q_{abs} are computed as described in [23]

$$\begin{cases} q_{em} = \frac{T_3 - T_4}{\Theta_{ref}} \\ q_{abs} = \frac{T_2 - T_1}{\Theta_{ref}} \end{cases} \tag{4}$$

  where $\Theta_{ref} = 8.15$ K/W

- T_c and T_h are derived by computing the temperature drop on the ceramic layers induced by the heat fluxes ($\Delta T = T_h - T_c$, $\bar{T} = (T_h + T_c)/2$)

$$\begin{cases} T_h = T_3 + q_{em}\Theta_{cer} \\ T_c = T_2 + q_{abs}\Theta_{cer} \end{cases} \tag{5}$$

  where $\Theta_{cer} = 0.02$ K/W

- $V_{th} = \alpha_S \Delta T$ and R_{in} are derived using equation (1), applying a mixed least squares linear regression [43] to the acquired values I, V_L

- α_S is then obtained as ratio of V_{th} to ΔT

- Θ_{in} is computed using equation (6) already obtained in [23]

$$\Theta_{in} = \frac{2(T_h - T_c)}{\alpha_S I_{st}(T_h + T_c) - (q_{em} + q_{abs})} \tag{6}$$

Table 1: Rated specifications at matched load conditions for TES1-12730 Thermoelectric Module by Thermonamic

T_h **Hot side** [**K**]	ΔT_{max} [3] ~~**Cold side**~~ [**K**]	V_{max} **Voltage**[1] [**V**]	I_{max} **Current**[2] [**A**]	R_{max} **Resistance**[4] [Ω]
300	70	16.2	3.5	3.47
323	79	16.9	3.5	3.74

Notes:
[1] Maximum voltage at ΔT_{max} and respective T_h
[2] Maximum current to achieve ΔT_{max}
[3] Maximum temperature difference occurs at I_{max}, V_{max}, and $Q = 0$ W
[4] Maximum resistance rated at AC conditions

3.2. TEM module

The characterization was performed using a TES1-12730 from Thermonamic Electronics Corporation [22], a low-cost commercial module designed for cooling applications. The module has an area of 30x30 mm^2 and a thickness of 3.6 mm, with Alumina (Al2O3) ceramic wafers. Its performances are declared by the manufacturer for two different working conditions, reported in Table 1. Also a couple of performance curves that provide the user with the qualitative trend of some parameters when ΔT varies are reported.

For such parameters a 10% tolerance is given with respect to product specifications.

3.3. Data acquisition system

All the voltages have been acquired using a National Instruments (NI) USB-6361 X Series data acquisition (DAQ) board, with eight 16-bit fully differential analog input channels able to provide sample rates up to 2 MS/s for single-channel acquisitions and up to 125 kS/ch/s for eight-channel acquisitions [44], extended with a BNC2110 DAQ accessory.

The adopted sampling frequency $f_S = 160$ Hz guarantees that the settling time requirements for multichannel measurements are largely met for each measurement range and for different source impedances as reported in the datasheet. For the sake of clarity, all information relative to each data channel have been reported in Table 2.

Table 2: NI USB-6361 channels resume

<table>
<tr><th>Symbol</th><th>Source</th><th colspan="2">Description</th><th>Range (V)</th><th>Settling time (μs) [b]</th></tr>
<tr><td>V_L</td><td>Load</td><td colspan="2">Load voltage</td><td>± 10</td><td>1.5</td></tr>
<tr><td>V_S</td><td>R_S</td><td colspan="2">Shunt voltage</td><td>± 5</td><td>1.5</td></tr>
<tr><td>T_a</td><td>LM35A</td><td rowspan="6">Temperature</td><td>Room</td><td>± 1</td><td>1.5</td></tr>
<tr><td>T_{cj}</td><td>LM35A</td><td>Cold Junction</td><td>± 1</td><td>1.5</td></tr>
<tr><td>T_4</td><td>J-type ThC</td><td>Layer 4</td><td>± 0.1</td><td>8</td></tr>
<tr><td>T_3</td><td>J-type ThC</td><td>Layer 3</td><td>± 0.1</td><td>8</td></tr>
<tr><td>T_2</td><td>J-type ThC</td><td>Layer 2</td><td>± 0.1</td><td>8</td></tr>
<tr><td>T_1</td><td>J-type ThC</td><td>Layer 1</td><td>± 0.1</td><td>8</td></tr>
</table>

[b] ±15 ppm of Step (±1 LSB for Full Scale Step)

Firstly, the DAQ board has undergone a self-calibration procedure to reduce the relative standard uncertainties in the interval 0.0046 - 0.0079 % of the full-scale as reported in Table 3. The specifications given in the Table are obtained following the worst case rule [45], as specified in the DAQ datasheet [44].

3.4. Temperature Sensors

The temperatures of the stacked layers are acquired using four grounded J-type bare thermocouples by RS Pro, with 1 m wires and suitable for temperature measurement in the range 223 K to 523 K. The manufacturer also provides a standard tolerance for thermocouples "J" class 1 of ±1.5 K in the range 233 K to 648 K.

The cold-junction compensation, as well as the measurement of the temperature inside the climate chamber, are both performed using two LM35A sensors by Texas Instruments, which provide a typical accuracy of ±0.2 K at 300 K room temperature and a worst-case accuracy of ±0.5 K at 423 K.

Table 3: NI USB-6361 uncertainty specifications (as percentage of V_{FS}, at full scale)

V_{FS}	$u_r(G)_\%$	$u_r(O)_\%$	$u_r(INL)_\%$	$u_r(Q)_\%$	$u_r(DAQ)_\%$
0.1	0.0063	0.0031	0.00346	0.00044	0.0079
1	0.0038	0.0011	0.00346	0.00044	0.0053
5	0.0033	0.0009	0.00346	0.00044	0.0049
10	0.0029	0.0009	0.00346	0.00044	0.0046

4. Metrological Characterization

In general, in this discussion, the term *uncertainty* will be a shorthand for *standard uncertainty*, as defined in the GUM (clause 2.3.1). Also the definition of Type A and Type B uncertainties is that provided by the GUM (clauses 2.3.2 and 2.3.3).

The mathematical models for the relevant output quantities are not easy to treat analytically for three main reasons:

- The number of input uncertainty contributions is high ($n = 21$, considering Type A and B contributions)
- Models are complicated and involve many intermediate results with which uncertain quantities are combined
- α_S and R_{in} are measured by means of linear regression performed on measured voltages and currents that are, in turn, uncertain.

While the first and the second issue may be overcome by means of symbolic computation engines, the last one poses a methodological concern that cannot be addressed by straightforward application of the GUM approach [24]. In fact, while the voltage across the TEM is directly measured by DAQ board channel, the current is measured indirectly as the ratio of voltage and resistance on a shunt resistor; all three quantities involved introduce uncertainty contributions of which only Type B evaluations are available.

Such a complex statistical model, however, can be straightforwardly implemented in a suitable Monte Carlo Simulation, which is a powerful tool for uncertainty analysis, relieving from the need of complicated analytical computations. On the other hand, some pitfalls in the Monte Carlo approach must be avoided: in particular, the simulation implemented here does not follow the scheme described in GUM Supplement 1 and 2 [46, 47], since it has some recognized issues.

In short, the Supplement 1 method (extended by Supplement 2 for the case of multiple output quantities [48]) aims at evaluating the posterior distribution of

Table 4: Individual Monte Carlo runs for the sensitivity analysis

Class	Monte Carlo run	Uncertain quantities	Description
Thermal	#1	$DAQ(T_a)$	Type A and B on DAQ channel for ambient temperature
	#2	$LM35(T_a)$	Type B on LM35 for ambient temperature
	#3	$DAQ(T_j)$	Type A and B on DAQ channel for cold junction temperature
	#4	$LM35(T_j)$	Type B on LM35 for cold junction temperature
	#5	$DAQ(T)$	Type A and B on DAQ channel for thermocouples
	#6	TC	Type B on temperature from thermocouples
Electrical	#7	$DAQ(V_{Sh})$	Type B on DAQ channel for voltage on shunt resistor
	#8	$DAQ(R_S)$	Type B on shunt resistance
	#9	$DAQ(V_{Ld})$	Type B on DAQ channel for load voltage

the measurand, in a Bayesian sense, and reaches its goal with a straightforward propagation of state-of-knowledge distributions. This procedure is equivalent to a simplified Bayesian analysis, and as such can give inconsistent results, corresponding to an erroneous choice of the prior distribution of the measurements. Theoretical analyses of the approach are, for example, in [49–52], and practical examples of clearly unsatisfactory results obtained by this approach in common problems are, for example, in [51, 53].

In this paper, instead, the Monte Carlo approach is used to perform numerical sensitivity analysis, by simulating "physical" measurement errors in the input quantities, and propagating them through the mathematical model of the measurement system. In particular, one uncertainty contribution at a time is considered [28]. This method, sometimes called "one at a time" (OAT) [27], consists in performing a separate Monte Carlo run for each of the n uncertain input quantities. Each run results in a specific partial uncertainty $\hat{u}_i(y)$, generated by a single input uncertainty contribution. In the end, therefore, a set of n distinct partial uncertainties $\hat{u}_i(y)$ for the measurement model $y = f(x_1, x_2, \ldots, x_n)$ is computed.

This Monte Carlo algorithm has been implemented in the MATLAB environment. The evaluations under every considered value of ambient temperature and temperature gradient are performed in parallel to speed up the computation. To perform the OAT sensitivity analysis, in each run only a single uncertainty contribution has been activated, except from the last run where all contributions were active to compute the global combined uncertainty. To evaluate the contribution of each source in a meaningful way, individual uncertainty contributions have been grouped as in Table 4. Basically, for DAQ channels, Type A and Type B uncertainties have been combined as suggested in the GUM ([24], Clause 4.3.7, Example 2) so that a more compact representation of sensitivities could be given.

All Type A uncertainty contributions have been simulated with random errors drawn from normal distributions with zero mean and $\hat{u}_A(x_i)$ standard deviation. On the other hand, all Type B uncertainty contributions have been simulated with random errors drawn from uniform distributions with zero mean and range $2u_B(x_i)$, since no further detail was given by sensors and DAQ manufacturers.

It is also worth observing that the last three runs deal with measurement data that, following the mathematical model, are used for a mixed least squares regression (Section 3.1). This means that runs #7, #8 and #9 include the statistical contribution of 160 measurements each that, however, are independent of each other and, consequently, are independently perturbed in the Monte Carlo algorithm.

A clear and interesting way to compare the contribution of input uncertainties is to express the sensitivities as partial contributions to the total output variance. That is, as suggested by Sobol [54]:

$$u = \frac{u_i^2(Y)}{u^2(Y)} \tag{7}$$

where $\hat{u}_i^2(Y)$ are the output uncertainties from each OAT step and $\hat{u}^2(Y)$ is the total variance, estimated in the last Monte Carlo run.

Finally, as a simple yet effective validation step, for each output quantity y it has been verified that

$$\sum_{i=1}^{N_{run}} u_i^2(y) \simeq u^2(y) \tag{8}$$

where $u(y)$ is the standard uncertainty computed in the Monte Carlo run where all contributions are active. This verification step has also highlighted that correlations between uncertainty components are negligible.

5. TEM Parameters Results

5.1. Operating conditions

Measurements have been performed under different operating conditions of the TEM, defined by an equally spaced grid in the $(T_C, \Delta T)$ space for 283 K $\leq T_C \leq$ 323 K and 10 K $\leq \Delta T \leq$ 45 K. As discussed in Section 2, the T_C and ΔT steady states have been set by means of a PI controller and, thereafter, their values have been measured. Therefore, the uncertainty on the operating conditions themselves must be investigated before the sensitivity analysis can be carried out.

The Monte Carlo algorithm shows that the most critical of the two parameters is ΔT, resulting from the combination of two temperature measurements performed with thermocouples. The relative standard uncertainty $u(\Delta\hat{T})/\Delta\hat{T}$, in fact, rapidly grows as ΔT decreases under 15 K.

For example, by applying the DAQ board specification for $\Delta T = 45$K, the differential voltage is about 2.4 mV measured on a full scale range of 0.1 V. The relative standard uncertainty is, in this case, about 40 times higher than at full-scale range, and for lower values of ΔT it is even worse.

The trend, as shown in Figure 3, is the same for all T_c values. The uncertainty on T_c, on the other hand, obviously increases for low temperatures, however it does not rise over 1.2% even for T_c close to 283 K. This is also due to the fact that Θ_{cer} in Equation (5) is small, and so is the temperature drop on the ceramic layers.

This preliminary analysis suggests in which region of the investigated steady states the uncertainty evaluation can give consistent results. Conventionally, results will be given for ΔT values whose uncertainty is not greater than $\sim 10\%$, i.e. $\Delta T \geq 12$ K.

This does not invalidate at all the characterization procedure, since the TEM used as Devices Under Test are commonly designed to be operated when the

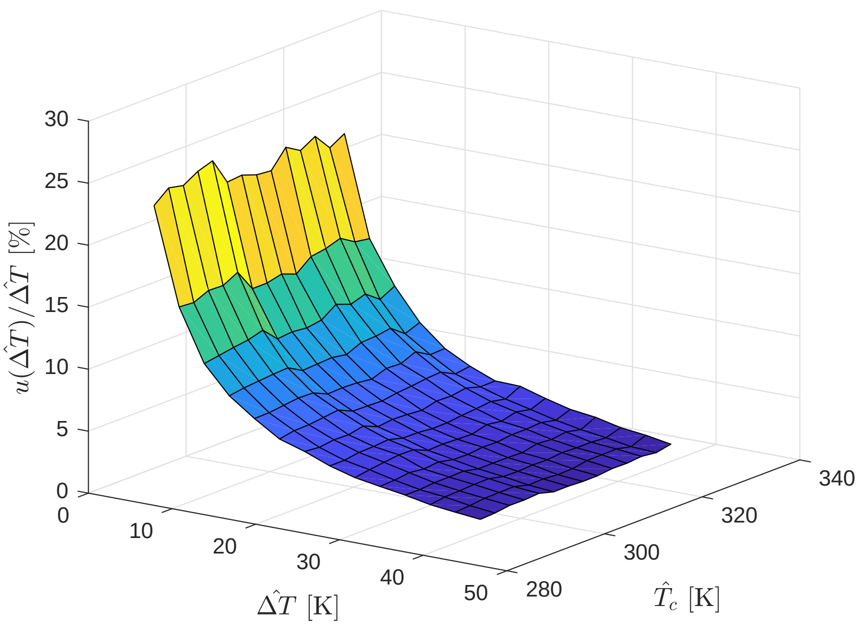

Figure 3: Relative uncertainty on ΔT measurements in the $(T_c, \Delta T)$ space

temperature gradient is in the order of some from few tens up to hundreds Kelvin degrees [22, 23].

Nevertheless, it is worth examining the uncertainty contributions to ΔT measurements in slightly more detail:

- Thermocouple coefficients ($\sim 78.45\%$ of total variance)

- DAQ measurements on 4 separate channels ($\sim 21.55\%$ of total variance)

Among the two, the effect of thermocouple coefficients is predominant. It is an exclusively sensor-related contribution, suggesting that using more accurate sensors than thermocouple would allow achieving significant results from the characterization procedure also for lower values of ΔT than those discussed in the next Section.

5.2. Sensitivity analysis

In this Section, the results from OAT sensitivity analysis are presented. As thoroughly discussed in Section IV, ten MC runs have been performed, one for each input uncertainty contribution, plus a run with every contribution active at once.

The first result of the analysis is that five of the nine uncertainty components outlined in Table 4 give almost no contribution to the total output variance for every output parameter, i.e. their contribution is several orders of magnitude lower than the others. Therefore, only the relevant contributions will be shown in the following bar graphs for the sake of readability.

Moreover, for all the parameters that are measured with both SS and CS methods, an error figure will be given to represent how much the estimates coming from each method deviate from each other. Such error is computed, for all y outputs, as follows:

$$e_Y = \frac{\overline{\overline{|Y_{SS} - Y_{CS}|}}}{\max_{T_C,\Delta T} Y - \min_{T_C,\Delta T} Y} \tag{9}$$

where the double bar operator defines the average taken over both T_c and ΔT. The global range of Y is chosen as reference for this error figure.

One may also immediately observe that results obtained with the SS method appear more "irregular" than those coming from the CS method (see, e.g. the figure of merit $Z\bar{T}$ in Figure 8). This is a consequence of electrical parameters (V_{th} and R_{in}) being estimated by means of a linear regression computed on narrowly spaced points, that is exactly the shortcoming of the SS method.

As last remark, it can be shown that, on the $(T_c, \Delta T)$ space, the uncertainties shows relevant trends only with respect to ΔT for every output parameter. A slice of the mesh plot taken for a conventional value of T_c, therefore, contains all relevant information about how the uncertainties change in the space of operating conditions, also with enhanced readability. Thence, the experimental results will be presented as follows:

- Parameter values: mesh plots (283 K $\leq T_c \leq$ 323 K and 12 K $\leq \Delta T \leq$

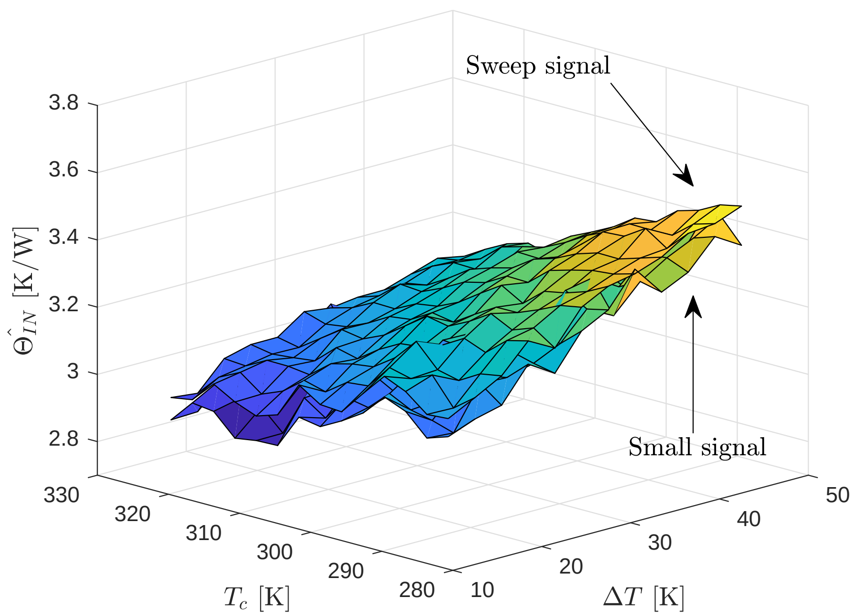

Figure 4: Thermal resistance of the TEM measured with both proposed methods ($e_{\Theta_{in}} = 0.21$)

45 K)

- Total relative uncertainties: 2D plots (T_c = 300 K and 12 K $\leq \Delta T \leq$ 45 K).

5.2.1. Θ_{in} thermal resistance

The SS and CS methods exhibit the same performance in terms of relative uncertainty and the maximum SS deviation from the CS value is less than 10%. This suggests that the proposed methods can be considered equivalent with respect to Θ_{in} measurement.

5.2.2. α_S Seebeck coefficient

As for Θ_{in}, the SS and CS methods exhibit the same performance in terms of total uncertainty, thermocouple coefficients giving the highest contribution. As visible in Figure 6(b), the Seebeck's coefficient measurement with the SS

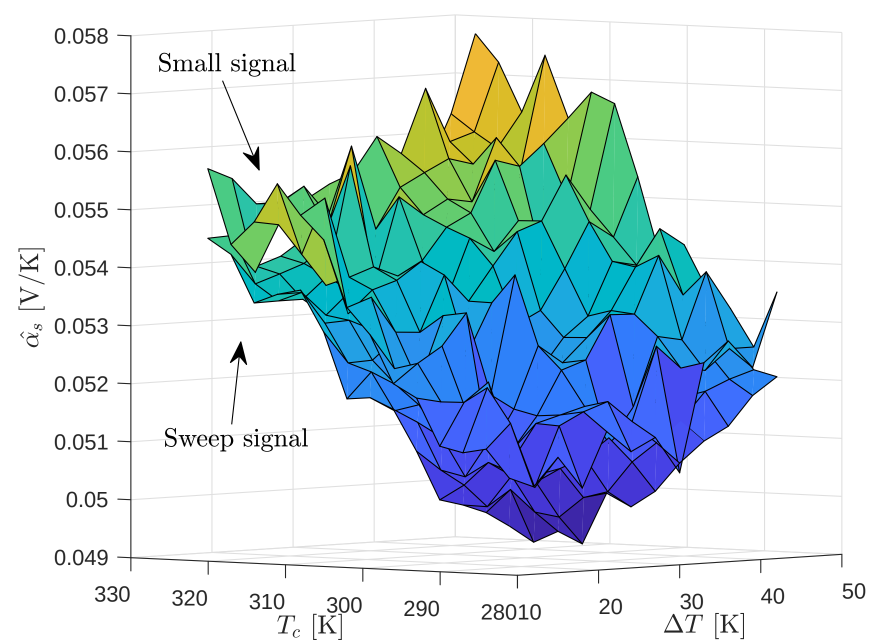

Figure 5: Seebeck coefficient measured with both proposed methods ($e_{\alpha_S} = 0.26$)

431 method is slightly more sensible to V_s and V_L uncertainties than Θ_{in}; this
432 difference propagates sensibly to $Z\bar{T}$ (Figure 9(a)).

433 *5.2.3. Seebeck voltage and electrical resistance*

434 These two parameters are computed from the same set of measurements,
435 thence they are hereby jointly discussed. Although, as shown in Figure 7, mea-
436 surement results provide sensibly different values in the operating conditions
437 space, the measurement model for both R_{in} and V_{th} does not directly depend
438 on any temperature measurement. The shunt resistor has been measured with
439 an Agilent 3458A 8½ digits multimeter, therefore its contribution to current
440 measurements can be neglected.

441 The outcome of the Monte Carlo analysis, on one hand shows that relative
442 uncertainties are low if compared to those affecting the other outputs, and on
443 the other hand, recalling the last paragraph of Section 5.2, they do not show
444 any visible trend as for Θ_{in}, α_S and $Z\bar{T}$, for the SS method. The uncertainties

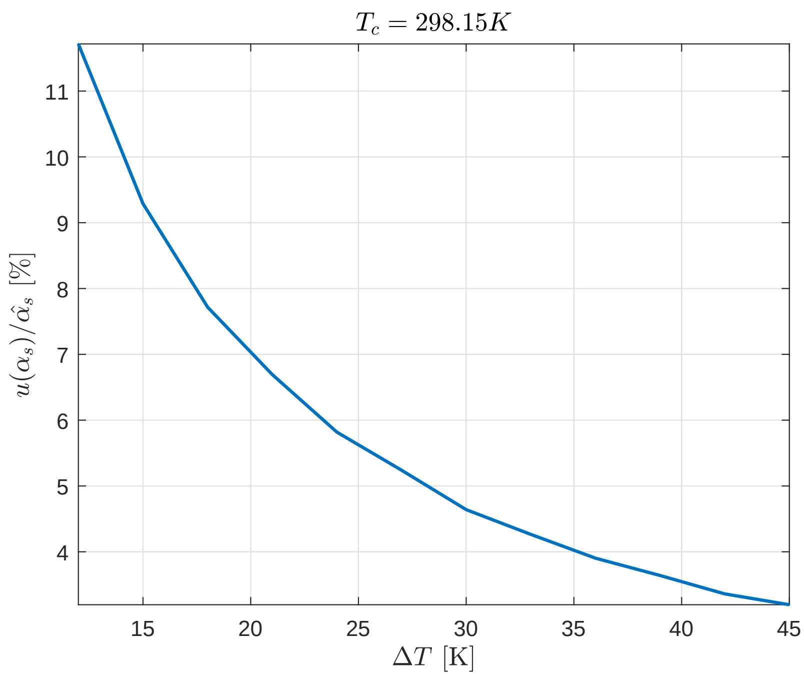

(a)

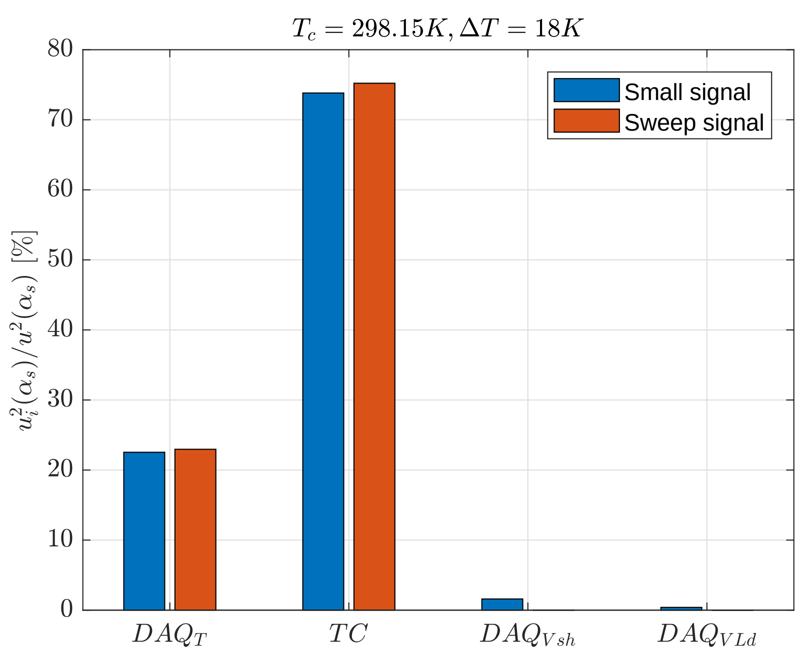

(b)

Figure 6: Relative uncertainty on α_S measurements (a) and uncertainty contributions from direct measurements as absolute standard uncertainties (b)

Table 5: Uncertainty evaluation for R_{in} and V_{th}

Parameter	**Error figure** [%]	**Method**	**Maximum uncertainty** [%]	**Average uncertainty** [%]
R_{in}	0.10	CS	0.01	0.01
		SS	0.63	0.01
V_{th}	0.03	CS	0.02	0.01
		SS	1.03	0.97

obtained from the CS method, instead, exhibit the same increasing trend as the other output parameters, plus a (way weaker) linear trend in the T_c direction. This may be due to the fact that the applied sweep signal was not fast enough to satisfy the steady state condition [55].

For these two parameters, results are expressed synthetically in Table 5, so that a global and comparative insight on the performance of the two methods is given. From the Table, it clearly appears that the two methods exhibit a good matching for R_{in}, but yield seemingly different estimates of V_{th}. The relative uncertainty on V_{th} is also two orders of magnitude greater for the SS method. This method, in fact, relies on measurement points that are much closer to each other than in the CS method, therefore the linear regression yields greater uncertainties.

5.2.4. $Z\bar{T}$ figure of merit

As already pointed out in [55], the linear dependence of the dimensionless figure of merit $Z\bar{T}$ is sensibly stronger on ΔT than on T_C (Figure 8). The CS method exhibits lower total uncertainty, enhancing this feature for high ΔT. This is clearly shown in Figure 9(a).

Looking at the sensitivity analysis (Figure 9(b)), the CS method is substantially insensitive to V_s and V_L uncertainties, while the contributions to $Z\bar{T}$ total uncertainty for the SS method come non-negligibly also from such measurements.

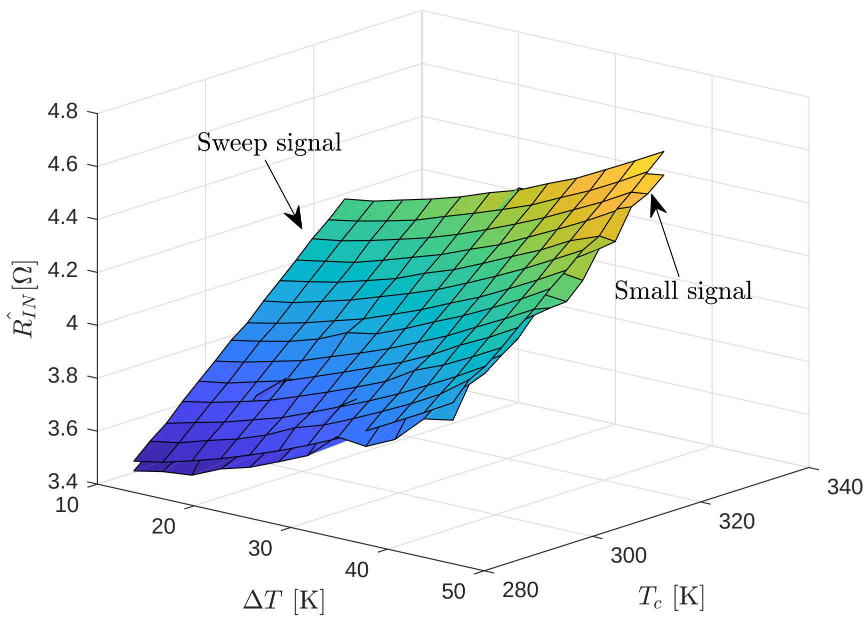

(a)

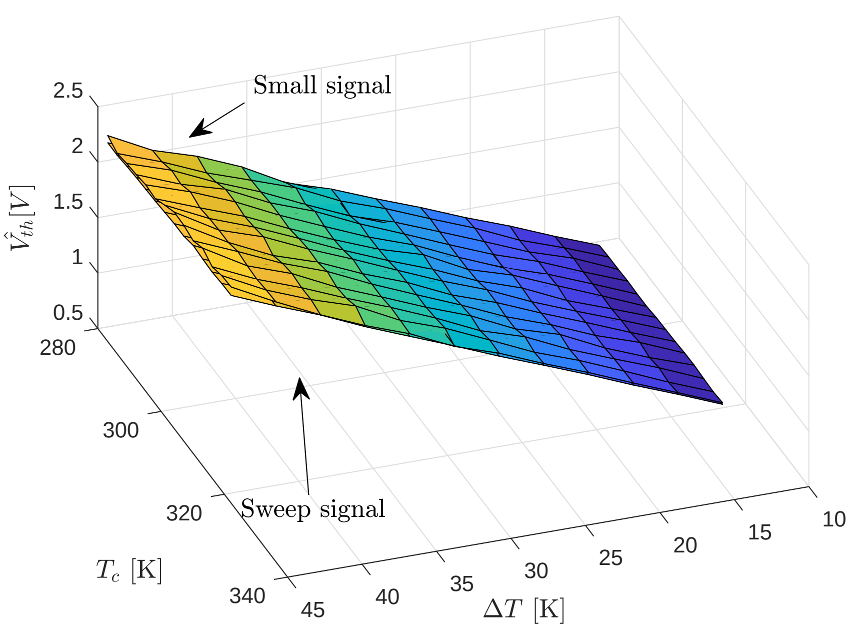

(b)

Figure 7: Electrical resistance R_{IN} (a) and Seebeck voltage V_{th} (b)

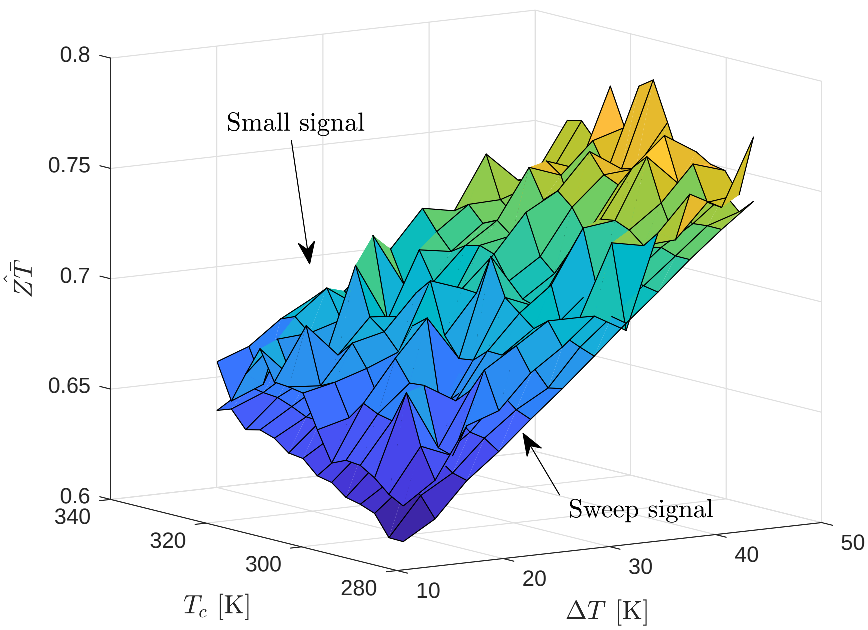

Figure 8: Dimensionless figure of merit $Z\bar{T}$ ($e_{Z\bar{T}} = 0.23$)

6. Conclusions

In this paper a methodology for the metrological analysis of the Unified Method for Thermo-Electric Module characterization has been developed and experimental results from a real testbed have been discussed. The individual uncertainty components have been outlined and a sensitivity analysis with respect to each component of the measurement setup has been performed with regard to both applied electrical stimuli.

The experimental results show that Current Sweep and Small Signal methods provide compatible estimates of every parameter and exhibit good results in terms of overall uncertainty, with Current Sweep performing better at the cost of employing more expensive and complex instrumentation. The sensitivity analysis, on the other hand, clearly highlights that the greatest contribution to overall uncertainty on the estimation of thermal parameters is given by temperatures measured with thermocouples, that are as a matter of fact widely employed in Thermo-Electric Module characterization practice.

~~Even so, the outcome of the sensitivity analysis points out that, if thermocouples are kept into the setup, cheaper acquisition devices can be employed without affecting the metrological performances~~

The results suggest that the proposed measurement setup can be dramatically improved by employing more accurate temperature sensors instead of standard thermocouples, without making any adjustment to the core characterization technique. By doing so, also Thermo-Electric Modules designed for low temperature gradients can be reliably characterized.

References

[1] Pérez-Izquierdo J, Sebastián E, M Martínez G, Bravo A, Ramos M and Rodríguez Manfredi J A 2017 *Measurement* ISSN 0263-2241 URL http://www.sciencedirect.com/science/article/pii/S0263224117307753

[2] Allmen L V, Bailleul G, Becker T, Decotignie J D, Kiziroglou M E, Leroux C, Mitcheson P D, Müller J, Piguet D, Toh T T, Weisser A, Wright S W and Yeatman E M 2017 *IEEE Transactions on Industrial Electronics* **64** 7284–7292 ISSN 0278-0046

[3] Andria G, Cavone G, Carducci C G C, Spadavecchia M and Trotta A 2016 A PWM temperature controller for themoelectric generator characterization *2016 IEEE Metrology for Aerospace (MetroAeroSpace)* pp 291–296

[4] Solbrekken G L, Yazawa K and Bar-Cohen A 2008 *IEEE Transactions on Advanced Packaging* **31** 429–437 ISSN 1521-3323

[5] Li C, Jiao D, Jia J, Guo F and Wang J 2014 *IEEE Transactions on Industry Applications* **50** 3995–4005 ISSN 0093-9994

[6] Reznikov M and Wilkinson P 2014 *IEEE Transactions on Industry Applications* **50** 4233–4238 ISSN 0093-9994

[7] Aranguren P, Araiz M, Astrain D and Martínez A 2017 *Energy Conversion and Management* **148** 680–691 ISSN 0196-8904 URL http://www.sciencedirect.com/science/article/pii/S019689041730585X

[8] Attivissimo F, Di Nisio A, Lanzolla A M L and Paul M 2015 *IEEE Transactions on Instrumentation and Measurement* **64** 1158–1169 ISSN 0018-9456

[9] Li Y, Yu H, Su B and Shang Y 2008 *IEEE Sensors Journal* **8** 678–681 ISSN 1530-437X

[10] Zoller T, Nagel C, Ehrenpfordt R and Zimmermann A 2017 *IEEE Transactions on Components, Packaging and Manufacturing Technology* **7** 1043–1049 ISSN 2156-3950

[11] Dalola S, Ferrari V, Guizzetti M, Marioli D, Sardini E, Serpelloni M and Taroni A 2009 *IEEE Transactions on Instrumentation and Measurement* **58** 1471–1478 ISSN 0018-9456

[12] Korhonen I and Lankinen R 2014 *Measurement* **58** 241–248 ISSN 02632241 URL http://linkinghub.elsevier.com/retrieve/pii/S026322411400356X

[13] Adamo F, Attivissimo F, Carducci C G C and Lanzolla A M L 2015 *IEEE Sensors Journal* **15** 2514–2522 ISSN 1530-437X

[14] Brunelli D, Passerone R, Rizzon L, Rossi M and Sartori D 2016 *Sensors* **16** 57 URL http://www.mdpi.com/1424-8220/16/1/57

[15] Rizzon L, Rossi M, Passerone R and Brunelli D 2014 Energy neutral hybrid cooling system for high performance processors *International Green Computing Conference* pp 1–6

[16] Jose A, D'souza A, Dandekar S, Karamchandani J and Kulkarni P 2015 Air conditioner using Peltier module *2015 International Conference on Technologies for Sustainable Development (ICTSD)* pp 1–4

[17] Sayyad S Y and Wankhede U S 2015 Experimental Analysis on Vapour Compression-Thermoelectric Hybrid Refrigeration System *2015 7th International Conference on Emerging Trends in Engineering Technology (ICETET)* pp 82–84

[18] Sandoz-Rosado E and Stevens R J 2009 *Journal of Electronic Materials* **38** 1239–1244 ISSN 0361-5235, 1543-186X URL http://link.springer.com/article/10.1007/s11664-009-0744-0

[19] Carmo J P, Antunes J, Silva M F, Ribeiro J F, Goncalves L M and Correia J H 2011 *Measurement* **44** 2194–2199 ISSN 0263-2241 URL http://www.sciencedirect.com/science/article/pii/S0263224111002338

[20] Russel M K, Ewing D and Ching C Y 2013 *Applied Thermal Engineering* **50** 652–659 ISSN 1359-4311 URL http://www.sciencedirect.com/science/article/pii/S1359431112003523

[21] Izidoro C L, Ando Junior O H, Carmo J P and Schaeffer L 2016 *Measurement* ISSN 0263-2241 URL http://www.sciencedirect.com/science/article/pii/S0263224116000117

[22] Thermonamic Electronics(Jiangxi) Corp, Ltd Ther High Performance and High Reliable Solution - TES1-12730-English.pdf URL http://www.thermonamic.com/TES1-12730-English.pdf

[23] Attivissimo F, Guarnieri Calò Carducci C, Lanzolla A M L and Spadavecchia M 2016 *Sensors* **16** 2114 URL http://www.mdpi.com/1424-8220/16/12/2114

[24] Joint Committee for Guides in Metrology (JCGM) 2008 Evaluation of measurement data - Guide to the expression of uncertainty in measurement URL https://www.bipm.org/utils/common/documents/jcgm/JCGM_100_2008_E.pdf

[25] Ren X, Ding W, Long Z, Li W, Li F and Zhang G J 2016 *IEEE Transactions on Instrumentation and Measurement* **65** 1605–1613 ISSN 0018-9456

[26] Wübbeler G, Krystek M and Elster C 2008 *Measurement Science and Technology* **19** 084009 ISSN 0957-0233, 1361-6501 URL http://stacks.iop.org/0957-0233/19/i=8/a=084009?key=crossref.323bc8914d880a2599b95679b332ad34

[27] Saltelli A (ed) 2008 *Global sensitivity analysis: the primer* (Chichester, England ; Hoboken, NJ: John Wiley) ISBN 978-0-470-05997-5 oCLC: ocn180852094

[28] Cox M and Harris P 2006 Software Support for Metrology Best Practice Guide No. 6 - Uncertainty Evaluation Tech. Rep. DEM-ES-011 URL http://www.npl.co.uk/publications/software-suuport-for-metrology-best-practice-guide-no.-6.-uncertainty-evaluation.

[29] Adamo F, Attivissimo F, Di Nisio A and Spadavecchia M 2011 *IEEE Transactions on Instrumentation and Measurement* **60** 1613–1622 ISSN 0018-9456

[30] Mackey J, Dynys F and Sehirlioglu A 2014 *Review of Scientific Instruments* **85** 085119 ISSN 0034-6748 URL http://aip.scitation.org/doi/10.1063/1.4893652

[31] García-Cañadas J and Min G 2014 *The Review of Scientific Instruments* **85** 043906 ISSN 1089-7623

[32] Jacquot A, Pernau H F, König J, Nussel U, Bartel M and Jaegle M 2010 Measurement uncertainties in thermoelectric research

[33] Min G 2014 *Measurement Science and Technology* **25** 085009 ISSN 0957-0233 URL http://stacks.iop.org/0957-0233/25/i=8/a=085009

[34] Harman T C, Cahn J H and Logan M J 1959 *Journal of Applied Physics* **30** 1351–1359 ISSN 0021-8979, 1089-7550 URL http://scitation.aip.org/content/aip/journal/jap/30/9/10.1063/1.1735334

[35] RichardJ Buist 1995 Methodology for Testing Thermoelectric Materials and Devices *CRC Handbook of Thermoelectrics* (CRC Press) ISBN 978-0-8493-0146-9 URL http://www.crcnetbase.com/doi/abs/10.1201/9781420049718.ch18

[36] Gromov G, Kondratiev D, Rogov A and Yershova L 2001 Z-meter: Easy-to-use Application and Theory *Proc. of VI European Workshop on Thermoelectrics, Freiburg*

[37] Rauscher L, Fujimoto S, Kaibe H T and Sano S 2005 *Measurement Science and Technology* **16** 1054–1060 ISSN 0957-0233, 1361-6501 URL http://stacks.iop.org/0957-0233/16/i=5/a=002?key=crossref.0a95cffa4b1cb46c8978a81a5812f130

[38] Kolodner P 2014 *The Review of Scientific Instruments* **85** 054901 ISSN 1089-7623

[39] Zybała R, Schmidt M, Kaszyca K, Ciupiński u, Kruszewski M J and Pietrzak K 2016 *Journal of Electronic Materials* **45** 5223–5231 ISSN 0361-5235, 1543-186X URL http://link.springer.com/10.1007/s11664-016-4712-1

[40] Wang H, McCarty R, Salvador J R, Yamamoto A and König J 2014 *Journal of Electronic Materials* **43** 2274–2286 ISSN 0361-5235, 1543-186X URL https://link.springer.com/article/10.1007/s11664-014-3044-2

[41] McCarty R and Piper R 2015 *Journal of Electronic Materials* **44** 1896–1901 ISSN 0361-5235, 1543-186X URL https://link.springer.com/article/10.1007/s11664-014-3585-4

[42] Chimchavee W 2011 *Journal of Electronic Materials* **40** 707–715 ISSN 0361-5235, 1543-186X URL http://link.springer.com/article/10.1007/s11664-011-1523-2

[43] Van Huffel S and Vandewalle J 1991 *The Total Least Squares Problem: Computational Aspects and Analysis* Frontiers in Applied Mathematics

(Society for Industrial and Applied Mathematics) ISBN 978-0-89871-275-9 URL http://epubs.siam.org/doi/book/10.1137/1.9781611971002

[44] National Instruments NI-6361 Device Specification URL http://www.ni.com/pdf/manuals/374650c.pdf

[45] Fabbiano L, Giaquinto N, Savino M and Vacca G 2016 *Journal of Instrumentation* **11** ISSN 1748-0221 URL http://stacks.iop.org/1748-0221/11/i=02/a=P02001

[46] Joint Committee for Guides in Metrology (JCGM) 2008 Evaluation of measurement data - Supplement 1 to the "Guide to the expression of uncertainty in measurement" - Propagation of distributions using a Monte Carlo method URL https://www.bipm.org/utils/common/documents/jcgm/JCGM_101_2008_E.pdf

[47] Joint Committee for Guides in Metrology (JCGM) 2011 Evaluation of measurement data – Supplement 2 to the "Guide to the expression of uncertainty in measurement" – Extension to any number of output quantities

[48] Ramos P M, Janeiro F M and Girão P S 2016 *Measurement* **78** 397–411 ISSN 0263-2241 URL http://www.sciencedirect.com/science/article/pii/S0263224115004753

[49] Elster C and Toman B 2009 *Metrologia* **46** 261 ISSN 0026-1394 URL http://stacks.iop.org/0026-1394/46/i=3/a=013

[50] Attivissimo F, Giaquinto N and Savino M 2012 *Measurement* **45** 2194–2202 ISSN 0263-2241 URL http://www.sciencedirect.com/science/article/pii/S0263224112000371

[51] Willink R and White R 2012 Disentangling classical and Bayesian approaches to uncertainty analysis Tech. rep. Technical Report No. CCT/12-08 URL http://www.bipm.info/cc/CCT/Allowed/26/Disentangling_uncertainty_v14.pdf

[52] Elster C 2014 *Metrologia* **51** S159 ISSN 0026-1394 URL http://stacks.iop.org/0026-1394/51/i=4/a=S159

[53] Giaquinto N and Fabbiano L 2016 *Metrologia* **53** S65 ISSN 0026-1394 URL http://stacks.iop.org/0026-1394/53/i=2/a=S65

[54] Sobol I M 1993 *Mathematical Modelling and Computational Experiments* **1** 407–414 URL http://max2.ese.u-psud.fr/epc/conservation/MODE/Sobol%20Original%20Paper.pdf

[55] Attivissimo F, Nisio A D, Carducci C G C and Spadavecchia M 2017 *IEEE Transactions on Instrumentation and Measurement* **66** 305–314 ISSN 0018-9456

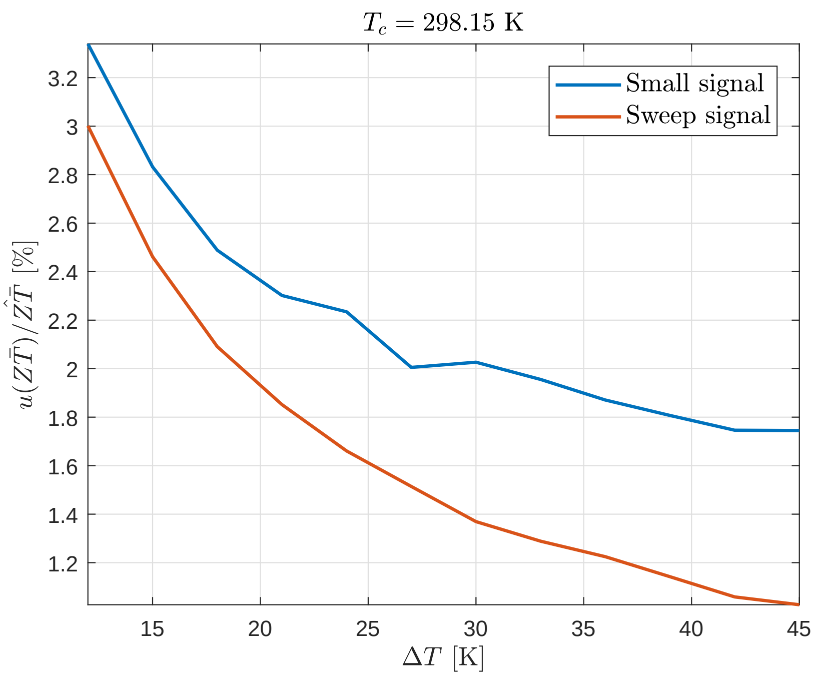

(a)

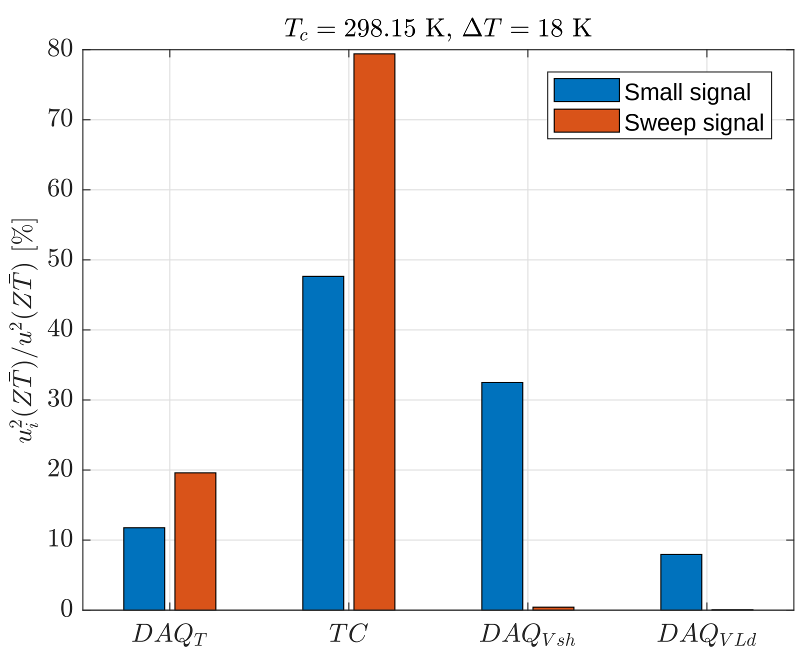

(b)

Figure 9: Relative uncertainty on $Z\bar{T}$ measurements (a) and uncertainty contributions from direct measurements as percentage of total variance (b)